Jurnal Teknologi

Full Paper

PREDICTION OF DISSOLUTION-INDUCED STRUCTURAL MODIFICATION IN LITHIUM ALUMINATE BORATE GLASS: COMPUTATIONAL MODELLING

Danial Ridzuan, Nor Ezzaty Ahmad*, Nik Muhammad Azim Nik Asni, Faizani Mohd Noor, Razif Razali, Suhairul Hashim, and Sib Krishna Ghoshal.

Department of Physics, Faculty of Science, Universiti Teknologi Malaysia, 81300 UTM Johor Bahru, Johor, Malaysia

Article history
Received
6 May 2025
Received in revised form
3 October 2025
Accepted
5 October 2025
Published Online
29 August 2026

*Corresponding author
norezzaty@utm.my

Graphical abstract

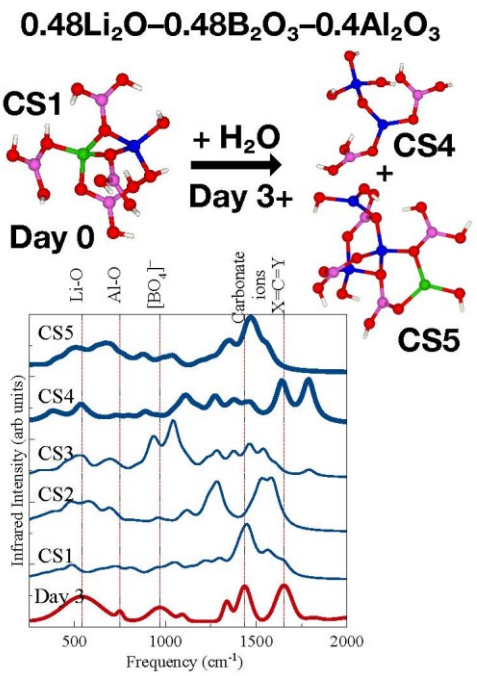

Abstract

Borate-based bioactive glass systems became interesting due to their faster degradation rate and better conversion into hydroxyapatite-like complex structures than silicate glasses. Unravelling the mechanism of structural modification and biomineralization in borate bioactive glass remains challenging. Thus, a computational model study was conducted to predict the dissolution-assisted structural changes in the lithium aluminate borate glass (LABG). The model simulation results were validated by the Fourier transformed infrared (FTIR) spectral analysis of LABG (of the form $0.48Li_2O$-$0.48B_2O_3$-$0.4Al_2O_3$) referred in [1]. Deionised water (DIW) dissolution-mediated changes in the molecular networks of the glasses were ascertained from the experimental FTIR band characteristics. The interaction of the glass network structures with DIW were determined by modelling five molecular clusters (in microcrystalline phase) matched to the experimental configuration. The selected clusters were based on the $Li_3Al(BO_3)_2$ crystal structure comparable to the experimental glass. The density functional theory (DFT) calculation on these optimized clusters was performed using Gaussian 09. The geometrical analyses were carried out at various dissolution periods (0, 3, 7 and 14 days) to compare with the experimental FTIR spectra. The glass after 3 days of dissolution showed the existence of two clusters accompanied by an ambiguous IR peak corresponding to the stretching vibration of $[BO_3]^{-2}$ together with two non-bridging oxygen. It was asserted that the proposed computational approach for the dissolution-enabled network structural modifications in LABG can be useful to predict various mechanisms in bioactive glass evolution.

Keywords: Bioactive Glass, Borate, FTIR, Gaussian, Computational

Abstrak

Sistem kaca bioaktif berasaskan borat menjadi menarik kerana kadar perlarutan yang lebih pantas dan keupayaan yang lebih baik untuk bertukar menjadi struktur kompleks seperti hidroksiapatit berbanding kaca silikat. Memahami mekanisme pengubahsuaian struktur dan biomineralisasi dalam kaca bioaktif borat kekal sebagai satu cabaran. Oleh itu, satu kajian model pengiraan telah dijalankan untuk meramalkan perubahan struktur yang dibantu pelarutan dalam kaca litium alumina borat (LABG). Hasil simulasi model ini disahkan melalui analisis spektrum inframerah transformasian Fourier (FTIR) kaca LABG (dalam bentuk $0.48Li_2O$-$0.48B_2O_3$-$0.4Al_2O_3$) seperti dirujuk

dalam [1]. Perubahan dalam rangkaian molekul kaca yang dimediasi oleh pelarutan air ternyahion (DIW) telah dikenal pasti daripada ciri jalur eksperimen FTIR. Interaksi struktur rangkaian kaca dengan DIW ditentukan melalui pemodelan lima kluster molekul (dalam fasa mikrohablur) yang sepadan dengan konfigurasi eksperimen. Kluster yang dipilih berdasarkan struktur hablur $Li_3Al(BO_3)_2$ yang setanding dengan kaca eksperimen. Pengiraan teori fungsian ketumpatan (DFT) ke atas kluster yang dioptimumkan ini dilakukan menggunakan perisian Gaussian 09. Analisis geometri dijalankan pada pelbagai tempoh pelarutan (0, 3, 7, dan 14 hari) untuk dibandingkan dengan spektrum FTIR eksperimen. Kaca selepas 3 hari pelarutan menunjukkan kewujudan dua kluster yang disertai dengan puncak IR yang taksa, merujuk kepada getaran peregangan $[BO_3]^{-2}$ bersama dua oksigen yang tidak menyambung (non-bridging oxygen). Hasil kajian menegaskan bahawa pendekatan pengiraan yang dicadangkan untuk pengubahsuaian struktur rangkaian yang dimediasi pelarutan dalam LABG boleh digunakan untuk meramal pelbagai mekanisme dalam evolusi kaca bioaktif.

Kata kunci: Kaca Bioaktif, Borat, FTIR, Gaussian, Pengiraan

1.0 INTRODUCTION

Bioactive glass or Bioglass® can be classified based on silicate (SiO_2), phosphate (P_2O_5) and borate (B_2O_3)-based glass formers [2]. Most of the researchers modified the composition of the precursor Bioglass® without changing these former oxides because of their rapid bonding to bone gives early mechanical stability as well as stimulating osteoprogenitor cell function and biocompatibility [3], [4], [5], [6], [7]. P_2O_5 glasses may be both bioactive and bioresorbable, however previous research has proved that their bioactive behaviour is insufficient compared to other glass with different former [8]. Despite their better bioactive properties than silicate glasses, borate-based glasses are less studied compared to other bioactive glasses [9]. Borate glasses can turn to calcium phosphate more rapidly during the process of cell proliferation and differentiation than the well-known Bioglass® 45S5 (made of 45 wt% of SiO_2, and 5 to 1 molar ratio of Ca to P) [8].

The network modifiers, are commonly composed of alkali and alkaline earth oxides and their function is to break down the glass network by forming non-bridging oxygen [10]. Lithium is one of a good modifier which has been widely used to support glass network because of its advantages in the promotion of thermal stability and chemical durability [11]. In addition, lithium can enhance the process of bone regeneration [12]. Meanwhile, intermediate oxides can be either network former or modifiers depending on the glass composition [10]. For instance, aluminium oxides, by exterminating several of the non-bridging oxygen, aluminium is commonly recognized as a stabilizer for glass [13]. It can strengthen the structure of the glass yielding better durability. The FTIR spectra LAB bioactive glass were examined [1] to understand the bond vibrations and existence of chemical functional groups responsible for bioactivity. However, the details of the molecular network structures and IR peak properties were not reported [1]. To get a fundamental insight regarding the dissolution-mediated structural changes referred in [1], it is essential to examine the network configuration of LABG especially when interacting with water molecules.

Repeated researches revealed that the computational techniques can predict the atomistic details of the desired complex structures that are inaccessible experiments, thus supporting diverse experimental analyses of bioactive glasses [14], [15], [16], [17], [18], [19]. It is worth noting that the computer modelling and simulation can illustrate the details of glass network structures, providing valuable information on the configurations' characteristics and their various correlations. It was stated [20] that a calculation towards crystalline materials is commonly forthright to run whereas it is complicated to apply these to an amorphous material. Considering the immense significance of borate-based bioactive glass system, we used a combined experimental and computational approach to understand the mechanism of glass network structure modifications due to dissolution in deionized water (DIW).

2.0 METHODOLOGY

2.1 Reference Experiment

Experimental work by [1] on pre- and post-dissolution tests (for 3, 7 and 14 days) of Li_2O-Al_2O_3-B_2O_3 glass has yield a good data and discussion in terms of understanding its chemical durability. The dissolution tests were performed in DIW at temperature of 37 °C. However, an improvement could be made in predicting the glass structure itself and ascertain some peculiar spectroscopic experimental data obtained.

Figure 1 illustrates the FTIR spectra of LABG pre- and post-dissolution in DIW. Table 1 shows the FTIR band assignments and positions. Star-labelled FTIR peaks in LABG after dissolving in DIW for 3, 7 and 14 days are interesting. These peaks at approximately 1700 cm^{-1} were not quantified.

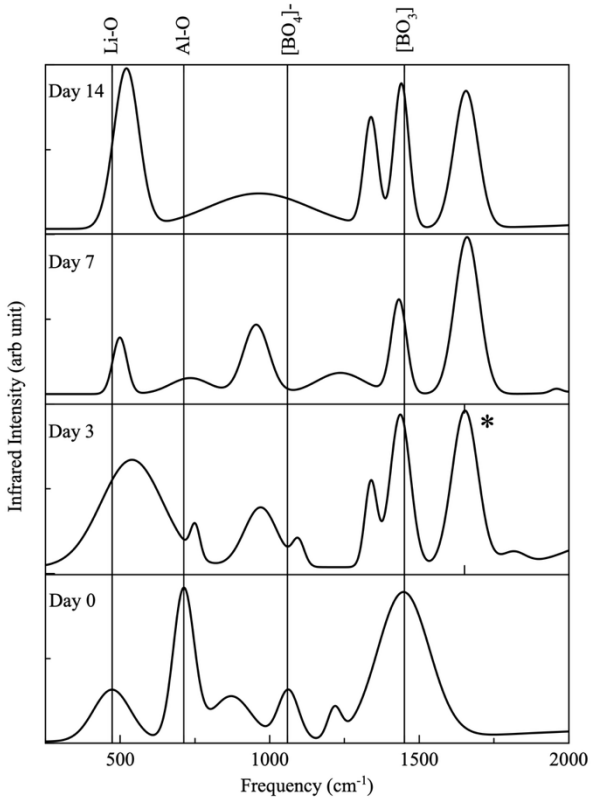

Figure 1 IR spectra of LABG before and after dissolution [1]

Table 1 FTIR spectral band assignments after dissolution process [1]

Vibration Groups	Band Position (cm^{-1}) and Dissolution Periods			
	Day 0	Day 3	Day 7	Day 14
Li-O bond or vibration of Li^+	418	542	506	527
Al-O bond AlO_6 octahedral units and AlO_4 tetrahedral units or bending vibration of B-O	713	715	734	753
B-O linkage of tetrahedral BO_4 units	973	1008	999	1078
B-O linkage of trigonal BO_3 units stretching	1486	-	-	-
Carbonate ions in apatite compounds	-	1431	1428	1437
X=C=Y various bonding	-	1649	1657	1644
O-H bonding	-	2218	2200	2190
O-H stretching	3423	3369	3344	333

2.1 Structural Optimization

In this study, LABG system composed of 0.48 mol% of Li_2O, 0.48 mol% of B_2O_3 and 0.4 mol% of Al_2O_3 was simulated to mimic earlier reported work [1]. Selected cluster structures were exported from CrystalMaker® software to Gaussview® 6.0.16 software [21] in Protein Data Base (PDB) format. The simulation was started with obtaining various crystal structures of borate from https://materialsproject.org database due to randomized structural configuration of glass. These structures were then divided into five molecular clusters (cluster structures) namely CS1, CS2, CS3, CS4 and CS5 according to the centre point of the cluster. Due to the complex structure of the origin crystal, the centre points exemplify the centre of distinct molecules for a single site of overall origin crystal. All calculations were performed using Gaussian® 09W. Optimizations were conducted for each cluster, with regard on balancing between the cost of calculation and the accuracy of the results obtained. The structural optimization provided minimal energy configuration of the molecules. The DFT calculations for the structures were carried out using APFD (Austin-Frisch-Petersson functional with dispersion correction) for CS1, CS2, CS3 dan CS4 clusters. However, CS4 cluster was optimized using Hartree-Fock calculation as it does not converge to the minimum level of energy using APFD. Furthermore, vibration spectra of LABG were computed to understand the experimental FTIR results. The selected clusters were based on the $Li_3Al(BO_3)_2$ crystal structure comparable to the experimental glass. Figure 2 displays the optimized structures for all clusters.

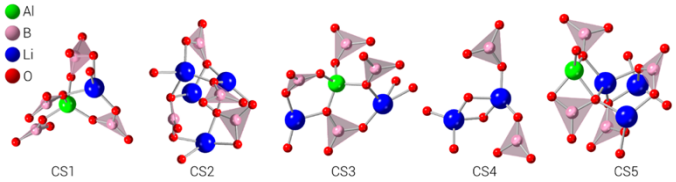

Figure 2 Optimized structure for cluster a) CS1, b) CS2, c) CS3, d) CS4 and e) CS5

3.0 RESULTS AND DISCUSSION

3.1 Optimum Structures

Calculations showed that Al_{10} atom was linked with four bridging oxygen (BO) with bond length in the range of 1.72 to 1.83 Å (Figure 2a). Meanwhile, [AlO_4] tetrahedra consisted of O-Al-O linkage with average bond angle of 109.5°. The O-Li-O tetrahedral angle range was widely varied in the range of 80.1° to 130.3° and its bond length was almost consistent at approximately 1.9 Å. Bond lengths of all trigonal B-O in [BO_3] were within range of 0.9 to 1.5 Å. The trigonal planar orientation had an angle of 121.3° that was close to the theoretical value 120° [13]. The angle of O_5-B_{11}-O_{18} was 128.1° that slightly differed from the

theoretical value which may be due to the bond breaking between H_{28} and O_{15} atoms.

Figure 2b shows the length of BO connected with Li_{10} which was approximately 2.0 Å. The angles for trigonal Li_{10} were ranged from 105.0° to 118.0°. Generally, the bond lengths between boron atoms and oxygen across this cluster were ranged from 1.5 - 1.6 Å except for trigonal B_9 that varied from 1.3 to 1.4 Å. The angles between BO and boron atom that involved in the ring-like structure (B_{15} and B_9) were both 117°.

The lengths of oxygen bonds to tetrahedra Al_{15} were around 1.72 to 1.78 Å (Figure 2c). The shortest bond length was 1.72 Å for Al_{15} bonded to O_{21} that only connected it for a much simpler trigonal B_{17} molecule. The angles were varied from 1.07° to 1.14°. The bond lengths for Li_3 to three BO were somehow varied where its lowest value was 1.73 Å (Li_3-O_4) and the highest value reached to 1.93 Å (Li_3-O_{12}). This brings to the wide array of trigonal angle with 146.8° for the maximum angle and 98.34° as the minimum value. Li_5 bonds with two (BO)s and two (NBO)s at length from 1.82 Å to 1.95 Å. Then, it could be observed that the bond length for all boron atoms with either BOs or NBOs showed an average value of 1.35 Å.

Li_{11} atom is in trigonal shape and same goes to B_5 and B_{10} atoms (Figure 2d) wherein Li_7 existed in the tetrahedral geometry. Bond lengths were ranged from Li_{11} with BOs (O_9, O_{13} and O_{14}) were about 1.68 to 1.82 Å. Li_7 connected with one BO (O_{13}) and three NBO (O_2, O_3 and O_8) is ranged from 1.68 to 1.82 Å. For trigonal boron, both B_5 and B_{10} bond length were approximately 1.30 Å to 1.43 Å.

Supposedly, Al_8 is in the form of tetrahedral with three (BO)s (O_{22}, O_{11} and O_{24}) and one NBO (O_{10}) but there is an abnormal bonding created between Al_8 and B_{18} due to the optimization process (Figure 2e). The abnormal bonding is due to the geometric constraints imposed during optimisation. Same goes to Li_{20} and Li_{14} which supposedly build in the shape of trigonal pyramidal and tetrahedral shape respectively but changed to five coordinated system due to the optimization process as well. It can also be observed that all boron is in the form of trigonal planar except for B_{18}. Cluster structure of Li_2O-Al_2O_3-B_2O_3 glass have been optimized and analysed in term of geometrical properties. Table 2 displays a comparison of average bond length between calculation and theory for all clusters. It was concluded that all the clusters were admissible due to the consistency of bond length and small percentage difference with between both.

Table 2 Average bond length and % difference before dissolution in DIW (0 day)

Cluster	Unit	Bond	Average Bond Length (Å)	Theoretical Value (Å)	Exp Value (Å)	% Difference
CS1	[AlO_4]	Al-O	1.759	2.164	1.800 [15]	2
	[LiO_4]	Li-O	1.935	1.979	2.000 [16]	3
	[BO_3]	B-O	1.306	1.371	1.350 [20]	3
CS2	[LiO_3]	Li-O	1.689	1.873	1.889 [14]	7
	[LiO_4]	Li-O	1.885	1.979	2.000 [16]	5
	[BO_3]	B-O	1.512	1.371	1.350 [20]	12
	[BO_4]	B-O		1.477	1.477 [20]	2
CS3	[AlO_4]	Al-O	1.753	2.164	1.800 [15]	3
	[LiO_3]	Li-O	1.852	1.873	1.889 [14]	2
	[LiO_4]	Li-O	1.892	1.979	2.000 [16]	5
	[BO_3]	B-O	1.370	1.371	1.350 [20]	1
CS4	[LiO_3]	Li-O	1.735	1.873	1.889 [14]	8
	[LiO_4]	Li-O	1.831	1.979	2.000 [16]	8
	[BO_3]	B-O	1.368	1.371	1.350 [20]	1
CS5	[AlO_4]	Al-O	1.779	2.164	1.800 [15]	1
	[LiO_3]	Li-O	1.877	1.873	1.900 [14]	1
	[LiO_4]	Li-O	1.920	1.979	2.000 [16]	4
	[BO_3]	B-O	1.369	1.371	1.350 [20]	1

3.2 FTIR Spectral Analysis of LABG (Experiment Day 0 Against Calculated)

A comparison was made between the calculated vibrational data and Day 0 experimental FTIR result obtained by [1] (Figure 3). The comparison was done to match the vibrational peaks and identify the respected molecules. Therefore, the structures and geometries of the desired Day 0 glass could be predicted. Based on the comparison for all cluster models (Table 3), most of them showed a peak of Li-O vibration except for CS3 cluster. The best matching peak is asymmetric stretching of [LiO_4] made by CS5 cluster at 493.13 cm-1. Experimental data for peak 713 cm-1 has been indicated as either [Al-O] bonding or [B-O] bending vibration. Based on the computational analysis, three clusters i.e., CS3, CS4 and CS5 indicated the closest peaks at 703.48, 710.85 and 709.49 cm-1 respectively, referring to bending vibration in wagging form of [BO_3]. Only one cluster CS1 shows stretching vibration of AlO4 at around 731.10 cm-1. From this information, it could be summarised that peak assignment in [1] shows disagreement from the calculated data where it shall represent the B-O bending vibration.

Cluster models of CS1, CS3 and CS5 agreed that peaks within the range of 1040 up to 1060 cm-1 is yielded by O-H vibration compared to experimental data that stated they belong to [BO^{4-}]. Model calculation performed on CS1, CS3 and CS5 clusters also proved that trigonal planar of [BO_3] with bending vibration existed eminently inside the amorphous structure with peaks at 1445.39, 1468.17 and 1446.70 cm-1. In short, only CS1 model (Figure 3) has matched almost all FTIR experimental peaks and could be chosen as the predicted geometrical structure for

Li_2O-Al_2O_3-B_2O_3 glass (as reference glass). The discrepancies of the computed and measured peak may be due to anisotropy.

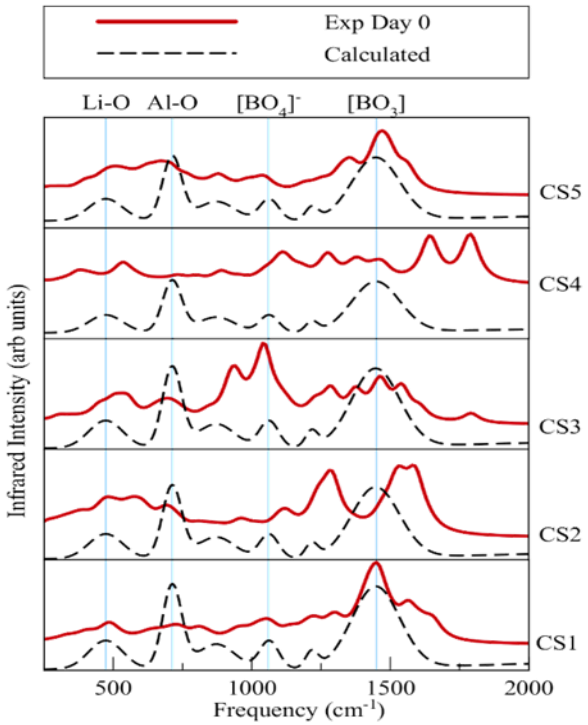

Figure 3 Calculated IR spectra at day 0 (red) of cluster CS1, CS2, CS3, CS4 and CS5 compared to experimental spectra of LABG from [1] (dotted-line)

Table 3 Comparison of experimental IR bands with computational prediction for each cluster after 3 days of dissolution in DIW

Expt. FTIR peak (cm^{-1})	Computed FTIR peak (cm^{-1})	Peak Assign (expt.)	Peak Assignment (computed)	Cluster Involved	Modes of vibration
473	382.61 463.13 389.52 493.13	Li-O	Li-O [LiO_4] Bonding	CS1, CS2, CS4 and CS5	Bending (Scissoring)
713	731.10 703.48 710.85 709.49	Al-O, B-O	B-O [BO_3] and Al-O [AlO_4] Bonding	CS1 (Al), CS3, CS4 and CS5	Bending (Wagging)
1060	1053.45 1044.63 1042.15	[BO^{4-}]	O-H Bonding	CS1, CS3 and CS5	Bending (Scissoring)
1450	1445.39 1468.17 1446.70	[BO_3]	O-B-O [BO_3] bonding	CS1, CS3 and CS5	Asymmetric Stretching and Scissoring Bending

3.3 Influence of Dissolution of Structural Modification of LABG

Figure 4 displays the calculated IR spectra at day 3 (blue) of cluster CS1, CS2, CS3, CS4 and CS5 compared to experimental spectra of LABG (dotted line) [1]. Clearly, some changes in the spectra occurred after the glass has undergo dissolution tests for 3 days. A new peak showed up within the range of 1600 to 1700 cm-1. According to [1], that peak was represented by carbonate covalent bond which however was not elaborated in detail. Also, most of all the other peaks are shifted from the original peak of Day 0 (Figure 3). Figure 4 assembles all the comparison between spectroscopic spectra of glass in day 3 and all calculated spectra. Based on the figure, it can be observed that only structure model of CS4 shows a few peaks within the interested range.

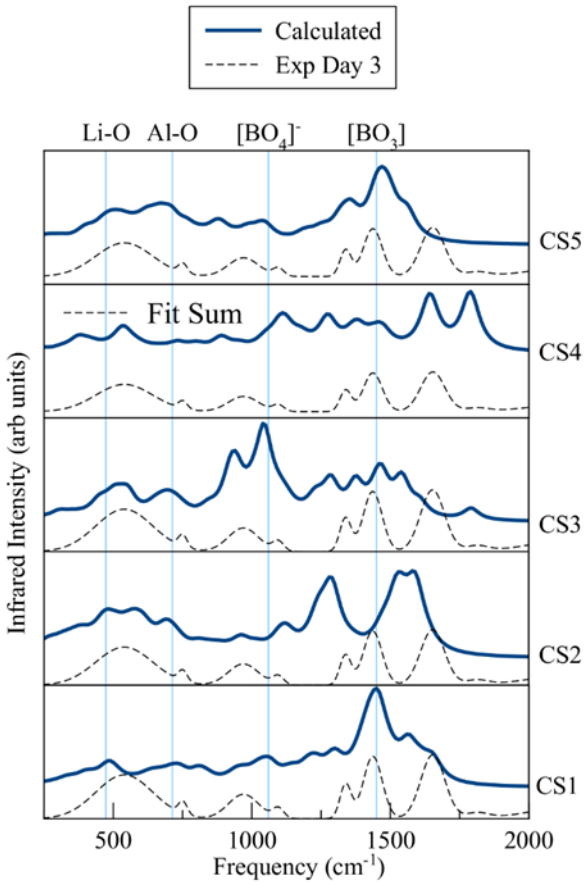

Figure 4 Calculated IR spectra at day 3 (dotted-line) of cluster (a) CS1, (b) CS2, (c) CS3, (d) CS4 and (e) CS5 compared to experimental spectra of LABG (blue) [1]

Based on the results in Table 3 and Table 4, it was observed that the bands starting from 1588.20 up to 1756.85 cm-1 were due to asymmetric stretching of O-B-O in trigonal planar of [BO_3]. Refer to Figure 2(d) above, boron atoms that involved both are boron with two NBO. We can see in Figure 1; the peak has continuously appeared along the next 14 days. It is proved that boron in form of boroxol ring and trigonal borate in three BO were breaks and changed into loose trigonal boron with two NBO.

The predicted structures represented a small part of the LABG that involved the DIW dissolution mechanism. The prediction before dissolution in DIW (day 0) agreed all IR spectral characteristics of CS1. While for dissolution in DIW for 3 days the glass structure was a combination of CS5 and CS4. The computationally simulated predicted structures of the LABG showed that the region of interest was referred to 3-coordinated boron with two NBO. It was asserted that the numbers of trigonal boron having two NBO were increased due to the dissolution process.

Table 4 Comparison of experimental IR bands with computational prediction for each cluster after 7 days of dissolution in DIW

Experimental FTIR (cm^{-1})	CS4 FTIR (cm^{-1})	Peak Assign (experimental)	Peak Assign (computed)	Modes of vibration
1653	1682.71	X=C=Y	B-O [BO3] Bonding	Stretching (Asymmetric)

Table 5 Comparison of computed IR peak assignment and vibration modes of CS4 with experimental spectra

Experiment FTIR (cm^{-1})	CS5 FTIR (cm^{-1})	Peak Assign (exp)	Peak Assign (computed)	Modes of vibration
530	493.13	Li-O vibration	Li-O [LIO4] Bonding	Stretching (Asymmetric)
750	765.29	Al-O vibration	Al-O [AlO4] Bonding	Bending (Wagging)
970	979.93	BO-4 vibration	B-O [BO3] Bonding	Stretching (Symmetric)
1435	1446.7	Carbonate ions	B-O [BO3] Bonding	Stretching (Symmetric)

4.0 CONCLUSION

The cluster structures of LAB bioactive glass were optimized, analyzed and predicted to determine the mechanism of DIW dissolution-induced structural modifications in the glass network, responsible for enhanced bioactivity. The computational results were validated with the experimental FTIR spectra of the LABG glasses for the first time. The results revealed that the clusters were admissible due to the consistency of bond lengths and percentage difference with the experimental FTIR data. A comprehensive comparison of the experimental FTIR spectra with the DFT calculation showed that most of the clusters matched to the experimental peaks, indication the region of interest peaks probed as asymmetric stretching vibration of O-B-O in trigonal planar of [BO_3]. The prediction before the dissolution in DIW indicated that the CS1 characteristics of the IR spectral peaks and after 3 days of dissolution the glass structure was a combination of CS5 and CS4. The proposed systematic approach may be useful for the development of LAB-based bioactive glasses needed for diverse biomedical applications.

Acknowledgement

This work is funded by the Ministry of Higher Education under Fundamental Research Grant Scheme (FRGS), Registration Proposal No: FRGS/1/2020/STG05/UTM/02/7.

Conflicts of Interest

The authors declare that there is no conflict of interest regarding the publication of this paper.

References

[1] Ali, N. F. M. 2019. *Structural and Durability Study of Lithium Aluminate Borate Glasses*. BSc thesis, Universiti Teknologi Malaysia.

[2] Baino, F., and C. Vitale-Brovarone. 2011. Three-Dimensional Glass-Derived Scaffolds for Bone Tissue Engineering: Current Trends and Forecasts for the Future. *Journal of Biomedical Materials Research Part A*. 97A(4): 514–535. https://doi.org/10.1002/jbm.a.33072.

[3] El-Ghannam, A., P. Ducheyne, and I. M. Shapiro. 1999. Effect of Serum Proteins on Osteoblast Adhesion to Surface-Modified Bioactive Glass and Hydroxyapatite. *Journal of Orthopaedic Research*. 17(3): 340–345. https://doi.org/10.1002/jor.1100170307.

[4] Ducheyne, P. 1998. Stimulation of Biological Function with Bioactive Glass. *MRS Bulletin*. 23(11): 43–49. https://doi.org/10.1557/S0883769400030992.

[5] Pazarçeviren, A. E., A. Tahmasebifar, A. Tezcaner, D. Keskin, and Z. Evis. 2018. Investigation of Bismuth-Doped Bioglass/Graphene Oxide Nanocomposites for Bone Tissue Engineering. *Ceramics International*. 44(4): 3791–3799. https://doi.org/10.1016/j.ceramint.2017.11.164.

[6] Khorami, M., S. Hesaraki, A. Behnamghader, H. Nazarian, and S. Shahrabi. 2011. In Vitro Bioactivity and Biocompatibility of Lithium-Substituted 45S5 Bioglass. *Materials Science and Engineering: C*. 31(7): 1584–1592. https://doi.org/10.1016/j.msec.2011.07.011.

[7] Tripathi, H., C. Rath, A. S. Kumar, P. P. Manna, and S. P. Singh. 2019. Structural, Physico-Mechanical and In Vitro Bioactivity Studies on SiO_2–CaO–P_2O_5–SrO–Al_2O_3 Bioactive Glasses. *Materials Science and Engineering: C*. 94: 279–290. https://doi.org/10.1016/j.msec.2018.09.041.

[8] Marion, N. W., W. Liang, G. C. Reilly, D. E. Day, M. N. Rahaman, and J. J. Mao. 2005. Borate Glass Supports the In Vitro Osteogenic Differentiation of Human Mesenchymal Stem Cells. *Mechanics of Advanced Materials and Structures*. 12(3): 239–246. https://doi.org/10.1080/15376490590928615.

[9] Brink, M., T. Turunen, R. P. Happonen, and A. Yli-Urpo. 1997. Compositional Dependence of Bioactivity of Glasses in the System Na_2O–K_2O–MgO–CaO–B_2O_3–P_2O_5–SiO_2. *Journal of Biomedical Materials Research*. 37(1): 114–121. https://doi.org/10.1002/(SICI)1097-4636(199710)37:1

[10] Fernandes, H. R., A. Gaddam, A. Rebelo, D. Brazete, G. E. Stan, and J. M. F. Ferreira. 2018. Bioactive Glasses and Glass-Ceramics for Healthcare Applications in Bone Regeneration and Tissue Engineering. *Materials*. 11(12): 2530. https://doi.org/10.3390/ma11122530.

[11] Rao, R. B., and R. A. Gerhardt. 2008. Effect of Alkaline Earth Modifier Ion on the Optical, Magnetic and Electrical Properties of Lithium Nickel Borate Glasses. *Materials Chemistry and Physics*. 112: 186–197. https://doi.org/10.1016/j.matchemphys.2008.05.046.

[12] Clément-Lacroix, P., *et al.* 2005. Lrp5-Independent Activation of Wnt Signaling by Lithium Chloride Increases Bone Formation and Bone Mass in Mice. *Proceedings of the National Academy of Sciences of the United States of America*. 102(48): 17406–17411. https://doi.org/10.1073/pnas.0505259102.

[13] Rabiee, S. M., N. Nazparvar, M. Azizian, D. Vashaee, and L. Tayebi. 2015. Effect of Ion Substitution on Properties of Bioactive Glasses: A Review. *Ceramics International*. 41(6): 7241–7251. https://doi.org/10.1016/j.ceramint.2015.02.140.

[14] Rada, S., E. Culea, and M. Neumann. 2010. Experimental and Theoretical Studies of the Structure of Tellurate-Borate Glasses Network. *Journal of Molecular Modeling*. 16(8): 1333–1338. https://doi.org/10.1007/s00894-009-0641-8.

[15] Rada, S., and E. Culea. 2009. FTIR Spectroscopic and DFT Theoretical Study on Structure of Europium-Phosphate-Tellurate Glasses and Glass Ceramics. *Journal of Molecular Structure*. 929(1–3): 141–148. https://doi.org/10.1016/j.molstruc.2009.04.021.

[16] Stoch, P., A. Stoch, M. Ciecińska, I. Krakowiak, and M. Sitarz. 2016. Structure of Phosphate and Iron-Phosphate Glasses by DFT Calculations and FTIR/Raman Spectroscopy. *Journal of Non-Crystalline Solids*. 450: 48–60. https://doi.org/10.1016/j.jnoncrysol.2016.07.027.

[17] Montazerian, M., E. D. Zanotto, and J. C. Mauro. 2020. Model-Driven Design of Bioactive Glasses: From Molecular Dynamics through Machine Learning. *International Materials Reviews*. 65(5): 297–321. https://doi.org/10.1080/09506608.2019.1694779.

[18] Alencar, V., J. Oliveira, A. Pereira, and S. Lucena. 2023. Molecular Simulation and Machine Learning Tools to Predict Bioglass Modulus of Elasticity. *Journal of Non-Crystalline Solids*. https://doi.org/10.1016/j.jnoncrysol.2023.122507.

[19] Lemm, D., G. F. von Rudorff, and O. A. von Lilienfeld. 2021. Machine Learning–Based Energy-Free Structure Predictions of Molecules, Transition States, and Solids. *Nature Communications*. 12: 4468. https://doi.org/10.1038/s41467-021-24525-7.

[20] Hasnip, P. J., K. Refson, M. I. J. Probert, J. R. Yates, S. J. Clark, and C. J. Pickard. 2014. Density Functional Theory in the Solid State. *Philosophical Transactions of the Royal Society A: Mathematical, Physical and Engineering Sciences*. 372 (2011). https://doi.org/10.1098/rsta.2013.0270.

[21] GaussView 6 Official Information Page. Accessed July 2, 2026. https://gaussian.com/gaussview6/